Correlation of multi-temporal ground-based optical images for landslide monitoring: Application, potential and limitations

J. Travelletti [a,b], C. Delacourt [c], P. Allemand [d], J.-P. Malet [a,*], J. Schmittbuhl [a], R. Toussaint [a], M. Bastard [a]

[a] Institut de Physique du Globe de Strasbourg, CNRS UMR 7516, Université de Strasbourg/EOST, 5 rue René Descartes, 67084 Strasbourg Cedex, France
[b] GEOPHEN – LETG, CNRS UMR 6554, Université de Caen Basse-Normandie, Caen, France
[c] Institut Universitaire Européen de la Mer, CNRS UMR 6538, Université de Bretagne Occidentale, Brest, France
[d] Laboratoire des Sciences de la Terre, CNRS UMR 5570, Université de Lyon and Ecole Normale Supérieure, Lyon, France

A B S T R A C T

The objective of this work is to present a low-cost methodology to monitor the displacement of continuously active landslides from ground-based optical images analyzed with a normalized image correlation technique. The performance of the method is evaluated on a series of images acquired on the Super-Sauze landslide (South French Alps) over the period 2008–2009. The image monitoring system consists of a high resolution optical camera installed on a concrete pillar located on a stable crest in front of the landslide and controlled by a datalogger. The data are processed with a cross-correlation algorithm applied to the full resolution images in the acquisition geometry. Then, the calculated 2D displacement field is orthorectified with a back projection technique using a high resolution DEM interpolated from Airborne Laser Scanning (ALS) data. The heterogeneous displacement field of the landslide is thus characterized in time and space. The performance of the technique is assessed using differential GPS surveys as reference. The sources of error affecting the results are then discussed. The strongest limitations for the application of the technique are related to the meteorological, illumination and ground surface conditions inducing partial or complete loss of coherence among the images. Small movements of the camera and the use of a mono-temporal DEM are the most important factors affecting the accuracy of the ortho-rectification of the displacement field. As the proposed methodology can be routinely and automatically applied, it offers promising perspectives for operational applications like, for instance, in early warning systems.

© 2012 International Society for Photogrammetry and Remote Sensing, Inc. (ISPRS) Published by Elsevier B.V. All rights reserved.

1. Introduction

Displacement monitoring of unstable slopes is a crucial tool for the prevention of hazards. It is often the only solution for the survey and the early-warning of large landslides that cannot be stabilized or that may accelerate suddenly. The choice of an adequate monitoring system depends on the landslide type and size, the range of observed velocity, the required frequency of acquisition, the desired accuracy and the financial constraints. Displacement monitoring techniques applied to landslides can be broadly subdivided in two main groups: geodetic and remote-sensing techniques.

Geodetic surveying consist in detecting geometrical changes in the landslide topography by measuring geometric parameters such as angles, distances or differences in elevation (e.g. levelling, tacheometry; Naterop and Yeatman, 1995). These techniques necessitate the installation of targets in and outside the landslide and in measuring their position at different times. They have the advantage to be very accurate (0.2–2.0 cm) with a high potential of automation (Malet et al., 2002; Jaboyedoff et al., 2004; Foppe et al., 2006). Furthermore, many authors demonstrated the efficiency of permanent (Malet et al., 2002) and non-permanent (Squarzoni et al., 2005; Brunner et al., 2007) differential Global Positioning System (dGPS) for landslide monitoring with a centimetric accuracy during any daytime and weather conditions. However, because landslides can show highly variable displacement rates in time and space according to the local slope conditions (bedrock geometry, distribution of pore water pressures), the major drawbacks of the geodetic techniques are (1) to provide only discrete point measurements of the displacement and (2) the costs of installation and maintenance of the survey network. They are usually only justified in the case of a real risk for the population.

Remote-sensing techniques are interesting tools to obtain spatially-distributed information on kinematics (Delacourt et al., 2007) and can be operational from spaceborne, airborne and ground-based platforms. Remote-sensing techniques give the

* Corresponding author.
  E-mail addresses: julien.travelletti@unistra.fr (J. Travelletti), jeanphilippe.malet@eost.u-strasbg.fr (J.-P. Malet).

possibility to discriminate stable and unstable areas and to map sectors within the landslide with different kinematics from a regional to a local scale. They are also useful tools for a process-based analysis of the deformation field affecting the slope (Casson et al., 2005; Teza et al., 2008; Oppikofer et al., 2008). In the last decades, the development of ground-based platforms for landslide monitoring at the local scale provided many advantages over spaceborne and airborne platforms despite a shorter spatial coverage (Corsini et al., 2006). The geometry and frequency of acquisitions are more flexible and adaptable to any type of local environment. In addition permanent installations of ground-based platforms allow continuous monitoring (Casagli et al., 2004; Delacourt et al., 2007). Three main categories of ground-based remote sensing techniques are used in landslide monitoring: Ground-Based Synthetic Aperture Radar Interferometry (GB-InSAR), Terrestrial Laser Scanning (TLS) and Terrestrial Optical Photogrammetry (TOP). A non-exhaustive review of the main advantages and disadvantages of these techniques is presented in Table 1. Detailed reviews of the application of GB-InSAR and TLS to landslides can be found in Corsini et al. (2006), Tarchi et al. (2003), Jaboyedoff et al. (2010), Teza et al. (2007, 2008) and Monserrat and Crosetto (2008). A state-of-the art of the application of TOP to landslide and related geomorphological processes is given below.

TOP is a technique with implementation, operating and equipment costs much lower than GB-InSAR and TLS. The technique consists in acquiring digital RGB images represented using a matrix of intensity values (brightness) recorded at each pixel of the Charge Coupled Device (CCD) of the camera from a spot very close to the ground (Jiang et al., 2008). In the last decades, camera self-calibration and analytical processing techniques allow the use of non-metric cameras and of simplified camera calibration algorithms to compute digital elevation models using the principle of stereoscopic views (Mikhail et al., 2001; Jiang et al., 2008). In the current state, the application of terrestrial images for landslide monitoring is mostly related to the production of DEMs for image ortho-rectification and sediment budget analysis (Bitelli et al., 2004; Pesci et al., 2004; Cardenal et al., 2008), and more recently to the characterization of the slope morpho-structure (Lim et al., 2005; Sturzenegger and Stead, 2009).

Using matching techniques, two-dimensional displacement fields can be derived by tracking objects in two images acquired at different time. So far, image correlation techniques have been applied only on aerial and satellite images (e.g. SPOT, QuickBird, OrbView, EROS) for the creation of landslide displacement maps (Casson et al., 2003; Delacourt et al., 2004; LePrince et al., 2008; Debella-Gilo and Kääb, 2011). The use of image correlation on terrestrial images has not been as popular for permanent landslide monitoring as in other application fields such as in solid and fluid mechanics for the characterization of the deformation pattern of soil/rock samples (White et al., 2003; Chambon et al., 2003; Küntz et al., 2007) or for the monitoring of other natural processes such as ice glaciers (Corripio, 2004; Fallourd et al., 2010; Maas et al., 2008) or volcanoes (Honda and Nagai, 2002). Only Delacourt et al. (2007) demonstrated an efficient application of TOP for landslide monitoring which consisted in the determination of the landslide boundaries and in the qualitative estimation of the spatial variability of displacement at the La Clapière landslide (French Alps) with an image acquisition system installed at 1-km distance.

Generally, the 2D displacements (in pixels) evaluated by the correlation algorithm have an accuracy of about 0.2 pixels (Casson et al., 2005; Delacourt et al., 2007) in the image plane, corresponding to an accuracy of millimeters to several centimeters for distances of about 100 m in the local coordinate system (Kraus and Waldhäusl, 1994).

The objective of this work is therefore to evaluate the potential and the limitations of TOP for the permanent monitoring of landslides using image correlation techniques. The dataset of images available for the Super-Sauze landslide (South French Alps) for the period 2008–2009 is used. First, the steps in the data acquisition and data processing (image correlation, ortho-rectification) are presented and the results are evaluated using the displacement of benchmarks measured by dGPS. Second, the main advantages and disadvantages of the method and the influence of external factors on the precision and the accuracy of the results are discussed.

Throughout this work, the accuracy is defined as the systematic difference between a measured quantity and the true value, and precision is defined as the random difference between multiple measurements of the same quantity.

Table 1
Relative advantages and disadvantages of GB-InSAR, TLS and TOP for landslide monitoring.

Techniques	Relative advantages	Relative disadvantages
GB-InSAR	High data accuracy possible (millimetric accuracy)	Requires large initial investment
	Monitoring during night and any type of weather conditions	Skilled crew required for operation
	Atmospheric effects can be corrected (permanent scatterers)	Displacement along line of sight
	Potential for high level of automation in acquisition and post-processing	Fails in detecting large and rapid displacements (signal decorrelation)
		Sensitive to changes in acquisition geometry and surface state variations
TLS	High data accuracy possible 1–4 cm (at 100 m range); 30 cm (at 1000 m range)	Requires large initial investment if buying
	Provides an easily understandable image	Skilled crew required for operation
	Potential for high level of automation in acquisition	Computation of the true 3D displacements require specific algorithms optimized for calculations on large 3D point clouds
		Large amount of computational resources for spatial data visualization
		Automated data post-processing difficult
TOP	High data accuracy possible from millimeters to a few centimeters at 100 m range	Adverse weather and illumination changes affect image quality
	Provides an easily understandable image	Not operating during the night
	Low initial and operating costs	Very sensitive to changes in acquisition geometry and surface state variations
	Low energy supply (passive sensors)	Ortho-rectification using accurate DEM is necessary for quantitative analysis
	Potential for high level of automation in acquisition and post-processing	Ground control points necessary for camera calibration
	Simple camera calibration	
	Simple matching algorithms available to produce DEMs and to compute 2D displacement fields	

2. Experimental site: the Super-Sauze landslide

To evaluate the potential of correlation of ground-based images for landslide monitoring, the dataset available at the Super-Sauze landslide, triggered in the Callovo-Oxfordian black marls of the South French Alps (Alpes-de-Haute-Provence, France; Fig. 1) is used. The landslide is located in the upper part of the Sauze torrential catchment. In the 1960s, the area was affected by rock falls in the scarp area. The fallen material composed of rocky panels progressively transformed into a silty-sandy matrix integrating marly fragments of heterogeneous sizes through successive weathering cycles (Malet, 2003). From the 1970s until today, the landslide material is gradually filling a torrential stream with a typical range of displacement rate comprised between 1 and 3 cm day^{-1} on average and possible acceleration of up to 40 cm day^{-1} (Malet et al., 2002). In 2007, the mudslide extents over a distance of 920 m between an elevation of 1980 m at the scarp and 1760 m at the toe with an average width of 135 m and a average slope of 25°. The total volume is estimated at 560,000 m^3 (Travelletti and Malet, 2012).

The kinematics of the landslide is currently monitored by differential Global Positioning System (dGPS), Terrestrial Laser Scanning (TLS) and by a remote camera monitoring system. This instrumentation consists in a low-cost D70 Nikon reflex digital camera installed on a concrete pillar located on a stable crest in front of the landslide at a distance of 300 m from the lower part and 900 m from the main scarp (Fig. 1A, B, and C). The acquisition system is controlled by a data logger (Campbell CR10) and the power is provided by a 40 W solar panel. The characteristics of the acquisition are presented in Table 2. Every four days, a series of images is acquired at 11:00, 12:00, 13:00 and 14:00 GMT in order to increase the probability of acquiring at least one image with good meteorological and illumination conditions. Each photograph (6 Mb) is stored in the Nikon native file format (NEF – Nikon Electronic Format) to avoid any loss of information.

3. Methodology

The steps in the data processing workflow consist in (1) correlating the images by pairs in their original acquisition geometry and (2) orthorectifying the calculated displacement fields using a high-resolution digital elevation model interpolated from airborne LiDAR data. The images presenting the best ground texture contrast and the most homogeneous lightening are manually selected. The detailed methodology is summarized in Fig. 2 and described below.

3.1. Principle of the image correlation technique

The 2D displacement field is obtained by correlating two optical images acquired at different time. The image correlation technique is based on the automatic identification of identical texture patterns within an image by maximizing a correlation function (Lewis, 1995; Baratoux et al., 2001; Debella-Gilo and Kääb, 2011). Its principle adapted for landslide kinematics analysis is described in (Delacourt et al., 2007). Visible ground features have to be superimposed on two successive images on stable parts located outside the landslide. On the areas affected by landslide movements, the visible and recognizable features are shifted by the displacements. In order to quantify the ground displacements, a correlation window is defined on a reference (often the oldest) image. The corresponding window is searched in a pre-defined explored area belonging to the second image. The starting point of this explored area is the expected position of the window with the assumption that no displacement occurred between two

acquisitions. The process is repeated for each pixel of the reference image. The Euclidean distance between the reference point and the matching point represents the displacement amplitudes in the image plane. By modifying the zone of interest, it is then possible to determine the displacements at various positions within the images. It is important to note that the normalized cross-correlation technique cannot track objects that start to rotate significantly or are affected by important perspective distortions (Lewis, 1995).

The size of the correlation window is a compromise between the desired accuracy on the displacement estimates and the spatial resolution of the velocity field (Delacourt et al., 2007). An increase of the size of the correlation window ensures a good signal to noise ratio and thus a good precision, but the accuracy on the displacement estimates decreases because of their averaging on a larger correlation window. This compromise is difficult to define when some parts of the landslide are well represented in terms of ground texture while other parts are not. Hierarchical correlation techniques allow one to overcome this problem by automatically changing the physical size of the correlation window and of the explored area during the correlation computations. The physical size is defined as the effective landslide surface covered by the correlation window (Rohály, 2002; El Alaoui and Ibn-Elhaj, 2009).

In this work, a sub-pixel hierarchical correlation technique is used (Hild, 2003; Chambon, 2003). The RGB images are first converted in gray-scale images to which a 3×3 pixel Sobel convolution matrix is applied to highlight the ground surface texture. The gradient values are then correlated (Chambon, 2003). Four successive degradations of the image resolution are applied following a pyramidal approach for changing the physical size of the correlation window and of the explored area by down-sampling the gradient values of the full resolution image (D'Antone, 1995; Kumar and Banerjee, 1998) (Fig. 3). The optimum sizes of the correlation window (16×16 pixels) and of the explored area (32×32 pixels) were identified with a trial and error procedure. These parameters are constant during the correlation computation. The correlation starts with the lowest resolution image in order to determine the largest displacements. Then the location of the pixel with the maximum cross-correlation value is used as the centre of the zone of interest for the next correlation step at a higher resolution. The spatial location of the maximum correlation value in the highest resolution image is thus progressively better estimated (Fig. 3). Ignoring high resolution information at the first computational step decreases the probability to reach a local minimum of the correlation function and, consequently, to obtain a wrong matching in the correspondence solution (El Alaoui and Ibn-Elhaj, 2009). In addition, this approach ensures very often a higher probability of detecting a reliable correlation peak (Anandan et al., 1993). The sub-pixel displacement is computed after the correlation at the highest resolution image. An iterative procedure is used to find the maxima of the correlation function interpolated with a bi-parabolic formula and with a maximization procedure based on the simplex method (Press et al., 1997; Chambon, 2003).

The correlation results consist in matrices of displacement Δu and Δv along the u- and v-axes in the image plane with their associated correlation index (Fig. 3). Because the pixel size is not constant in the image due to the oblique acquisition, the displacement field correlated in the image plane cannot be directly interpreted in terms of metric displacements. Therefore an orthorectification procedure is necessary for a quantitative analysis of the displacement fields.

3.2. Ortho-rectification of the displacement field using high-resolution digital elevation models (DEMs)

The orthorectification procedure consists in transforming the central projection of the image into an orthogonal view of the
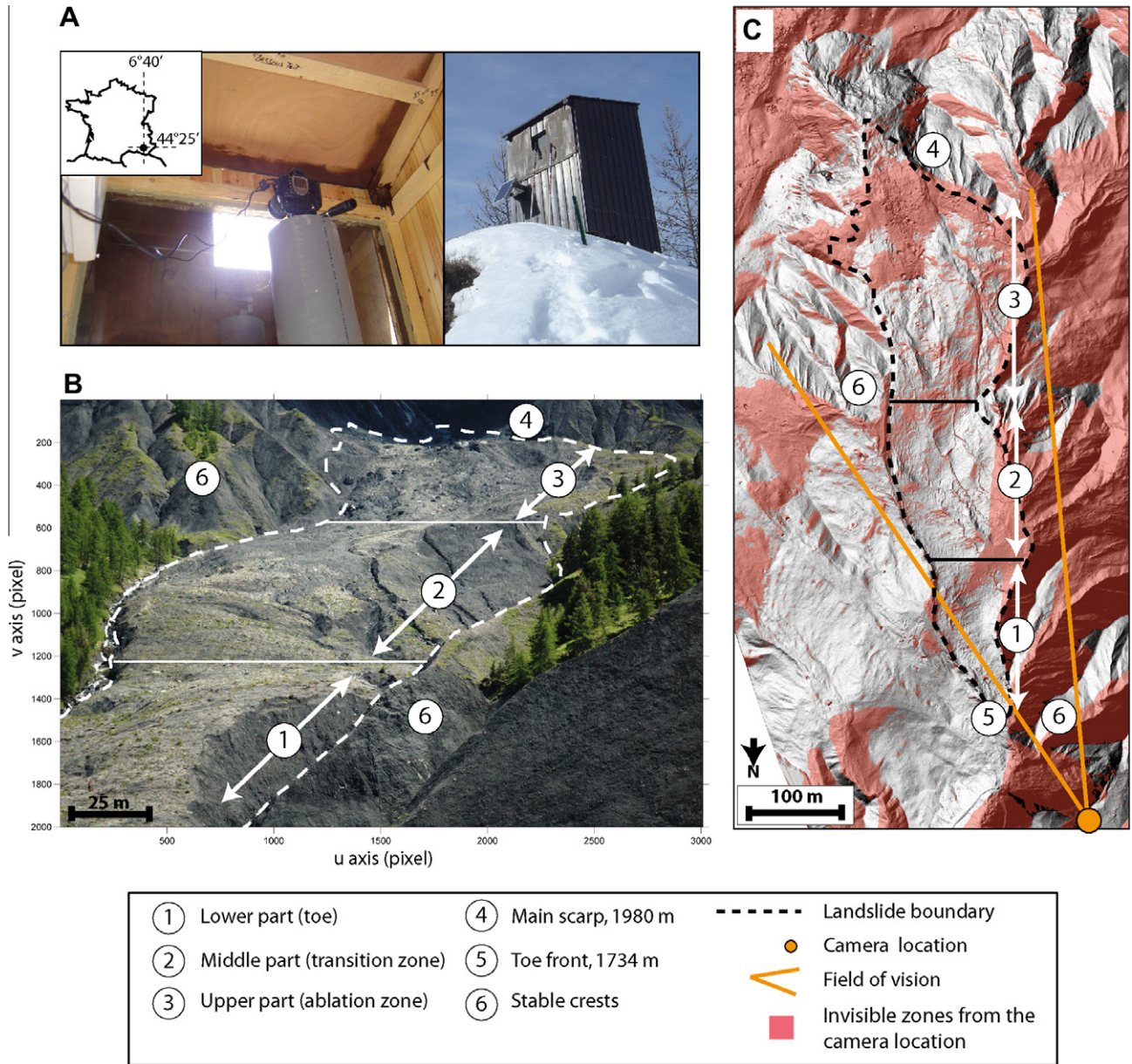
Fig. 1. Overview of the Super-Sauze landslide (South French Alps). (A) Monitoring system by terrestrial optical photography. (B) Image acquired by the monitoring system presenting the different parts of the landslide from the camera location. (C) View of the landslide morphology in the local coordinate system on a shaded relief computed with a 0.25 m resolution DEM interpolated from an airborne LiDAR survey (ALS) acquired in July 2009. The invisible areas from the camera location are indicated.

Table 2
Characteristics of the camera acquisition systems.

Type of camera	Single-lens reflex Nikon digital camera
Effective pixels	6.1 million
Image sensor	RGB CCD, 23.7 × 15.6 mm
Image size	3008 × 2000 pixels
Sensitivity	400 iso
Focal length	52 mm
Shutter speed	1/800
Storage media	CompactFlash™ (CF) Card
Storage system	NEF (Nikon RAW)

ground by correcting the effects of various distortion sources such as camera orientation, topographic effects and lens characteristics (Kraus and Waldhäusel, 1994). In terrestrial photogrammetry, distortions induced by topography effects are the most important due to the oblique acquisition of the images. The orthorectification converts the initial (u, v) and the final $(u + \Delta u, v + \Delta v)$ positions of the displacement vectors in a local coordinate system. The conversion is possible if a digital elevation model (DEM) of the object is available in order to relate two-dimensional pixel positions in the image plane to three-dimensional points in a local coordinate system using parametric approaches (Hemmleb and Wiedemann, 1997).

In our approach, the rotation angles defining the external orientation of the camera are first determined using the relationship between the image coordinates (u, v) and the local coordinate systems (X, Y, Z) given by the collinearity equations (Bonneval, 1972; Kraus and Waldhäusl, 1994). These equations are based on the principle that each point in the local coordinate system is projected with a straight line through the projection center (origin of the camera) into the image plane. Knowing the exact location of the camera and assuming that the principal point is at the center
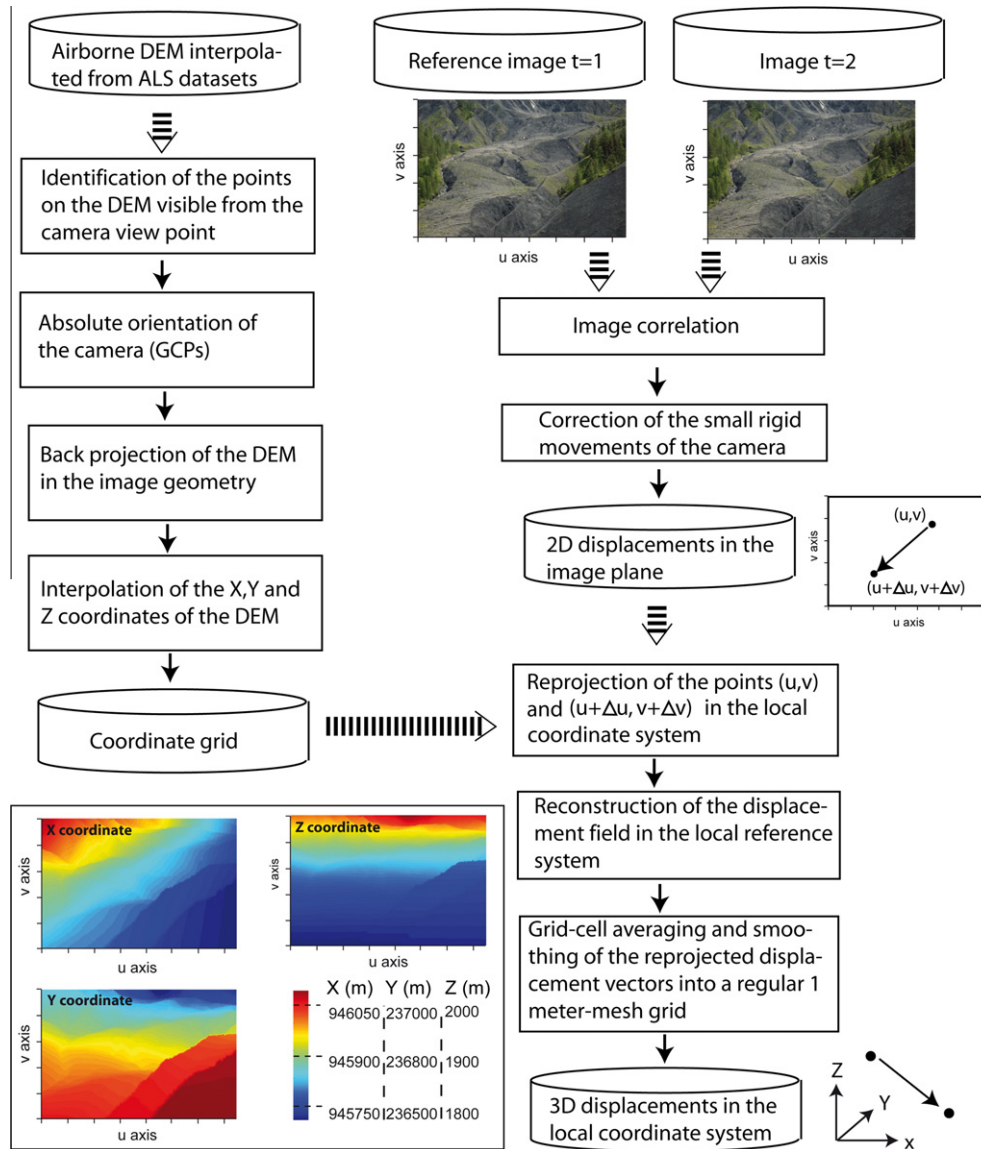
Fig. 2. Flowchart of the methodology.

of the image, the external angle and the effective focal length defining the absolute orientation and the internal parameter of the camera, respectively, can be determined with help of Ground Control Points (GCPs; Heikkila and Silven, 1997; Corripio, 2004).

In our case, a series of 95 pairs of GCPs distributed on the image plane and in the local reference system were measured with dGPS (Fig. 4). The centers of the GCPs are positioned in the local coordinate system with an average 3D accuracy of 0.02 m and a standard deviation of 0.01 m. The coordinates (u, v) of the GCPs in the image plane are determined by manual picking with an estimated accuracy of about 2 pixels. Among the 95 GCPs, 45 are used to compute the external parameters and 40 are kept to calculate the accuracy of the transformation (Section 5.2.1). A least mean square minimization technique based on a Direct Linear Transformation (DLT) and Singular Value Decomposition (SVD) between observed and calculated GCPs in the image plane is used to determine the external and internal parameters that satisfy the collinearity equations (Abdel-Aziz and Karara, 1971; Heikkila and Silven, 1997).

Then, two DEMs (0.25 m mesh-size, 3D error of 0.07 m) interpolated from Airborne Laser Scanning (ALS) dense point clouds acquired in October 2007 and July 2009 are used to orthorectify the displacements. A back projection of the DEMs is applied in the image plane using the external and internal parameters of the camera previously determined with the GCPs (Mikhail et al., 2001; Corripio, 2004). Only the points of the DEM visible from the camera viewpoint are back projected to avoid duplicate points in the same position in the image plane. The sightline method is used to identify the visible points (Fig. 1C; Fisher, 1991; Franklin and Rav, 1994). About 57% of the landslide area is visible from the camera view point. No displacements can be determined in the invisible areas. The 3D coordinates of the projected DEMs are then linearly interpolated in the image plane to allocate a triplet of X, Y, Z coordinates to each initial point (u, v) and each final point $(u + \Delta u, v + \Delta v)$ of the correlated displacements. A re-projection of the displacement vector components in the local reference system is then applied. The displacement components in the local coordinate system are finally averaged and smoothed in a regular grid with a mesh size of 1 m.

The use of a mono-temporal DEM for the orthorectification of the initial point (u, v) and the final point $(u + \Delta u, v + \Delta v)$ of the displacement vectors is a strong hypothesis that the global landslide morphology remains constant over the period. It affects the accuracy
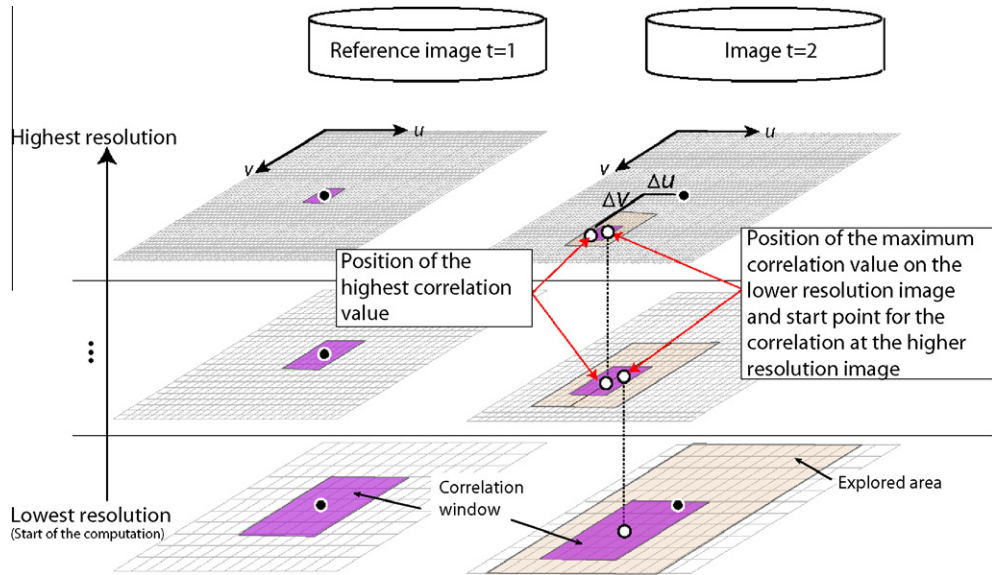
Fig. 3. Principle of normalized hierarchical image correlation.
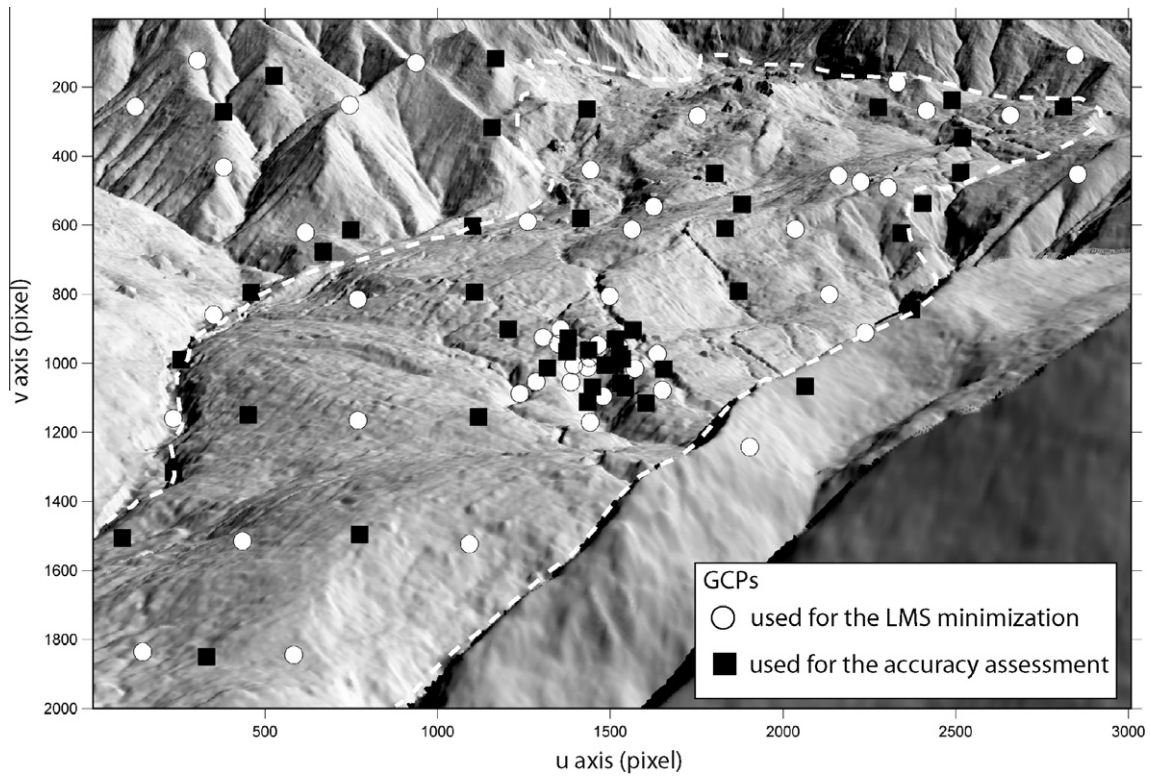
Fig. 4. Location of the Ground Control Points (GCPs), used for the Least Mean Square minimization (LMS) and for the accuracy analysis, plotted on a shaded relief image. The shaded relief image is produced by interpolating the shaded relief values of the ALS DEM of 2009 projected into the image plane.

of the transformation of the displacement vector in the local coordinate system. However, it will be further demonstrated that this method is still a relevant estimation for our purpose with reference to the amplitude of the observed displacements (Section 4.2).

3.3. Image resolution at the terrain surface

The effective (e.g. ground) pixel size is one of the limiting parameters for the accuracy of the correlation (Fig. 5A). It determines the minimum theoretical displacement that can be detected

for a pixel-level correlation. Below this displacement threshold, the accuracy solely depends on the accuracy of the sub-pixel correlation. The effective pixel size depends on (1) the distance between the object and the camera and (2) the angle of incidence which is defined as the complementary angle between the line of sight of the camera and the normal to the terrain surface (Fig. 5B). A low incidence angle means that the line of sight is nearly tangential to the topography.

Globally, the incidence angle on the landslide ranges from $0°$ to $40°$ and the pixel size varies from 1×10^{-2} m^2 in the lower part (at
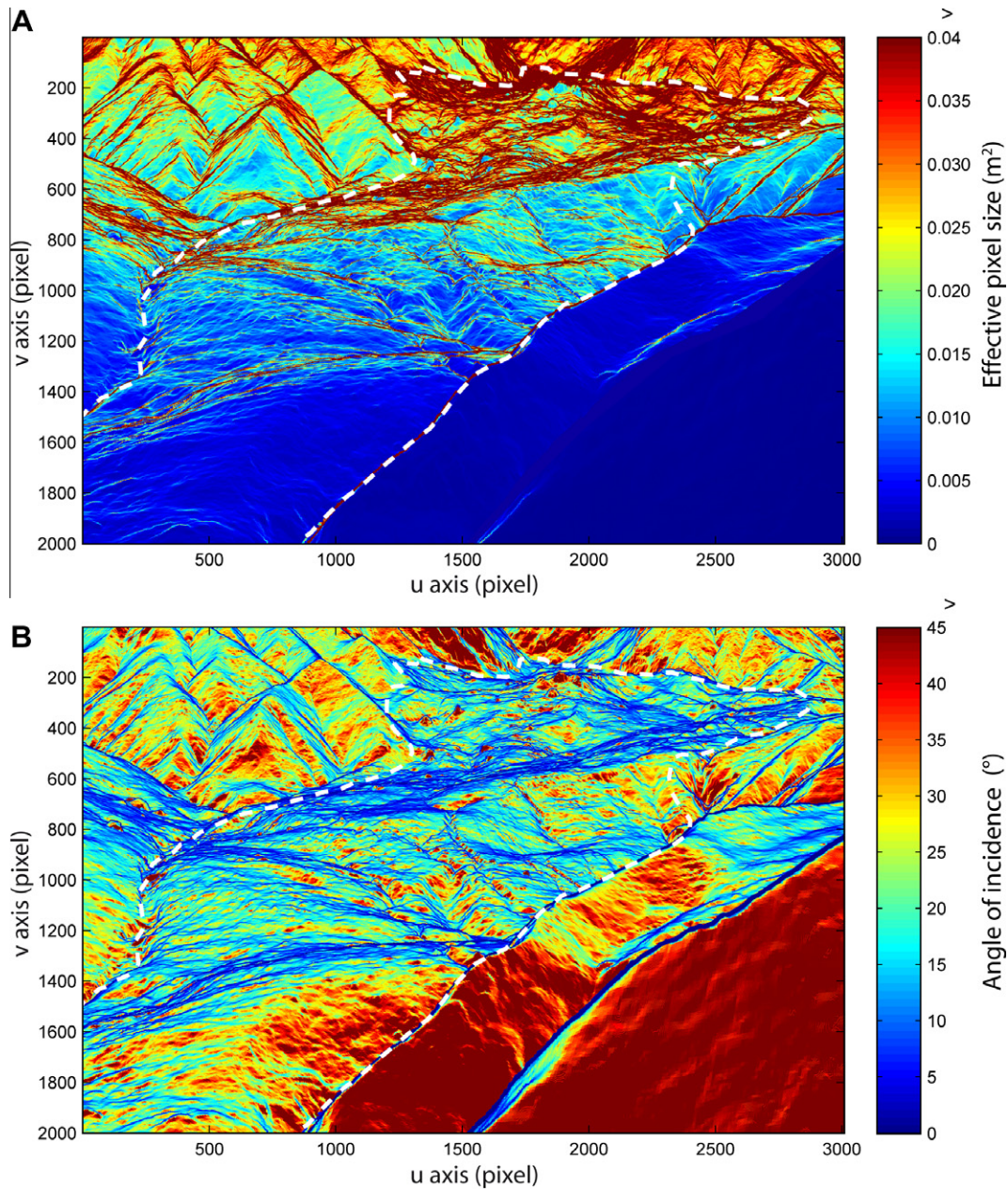
Fig. 5. Characteristics of the images: (A) Effective pixel size calculated with the ALS DEM of 2009 projected to image geometry (in m^2); (B) Angle of incidence (in degrees).

an average distance of 300 m) to 3×10^{-2} m^2 in the upper part of the landslide (at an average distance of 900 m; Fig. 5A and B). The upper part is characterized with a pixel size often larger than 0.04 m^2, especially in areas where the angle of incidence is less than 5°. Therefore the lowest accuracy is expected in this region because the detection of small Δv and Δu displacements can correspond to important ΔX, ΔY, ΔZ metric displacement. Approximately half of the number of pixels in the image plane inside the landslide area show a metric sensitivity of less than 0.17 m for 1 pixel displacement along the v-axis and of less than 0.07 m along the u-axis. The minimum displacements for a pixel-level correlation in the u and v-direction are 0.04 and 0.06 m, respectively, in the lower part of the landslide and 0.09 and 0.11 m in the upper part. In areas where the incidence angle is less than 5°, the minimum displacement that can be detected drastically increases. Therefore no strong confidence is given to areas whose incidence angle is lower than 5°.

3.4. Post-processing: displacement filtering

Filtering criteria are necessary to remove the badly correlated points and improve the signal to noise ratio (Casson et al., 2003; Berthier et al., 2005; Wangensteen et al., 2006; Debella-Gilo and Kääb, 2011). Three criteria are used in this work to filter aberrant displacements in the image plane coordinate system and in the local coordinate system. They are based on:

1. The value of the correlation peak coefficient: loss of coherence can occur during the computations because changes in surface states between a reference image and the correlated image are high, resulting thus in low correlation coefficients. Defining a threshold value has the consequence to increase the percentage of realistic displacements. A high threshold coefficient of $r = 0.6$ was selected to remove the badly correlated points. However, the correlation peak coefficient alone is not a sufficient
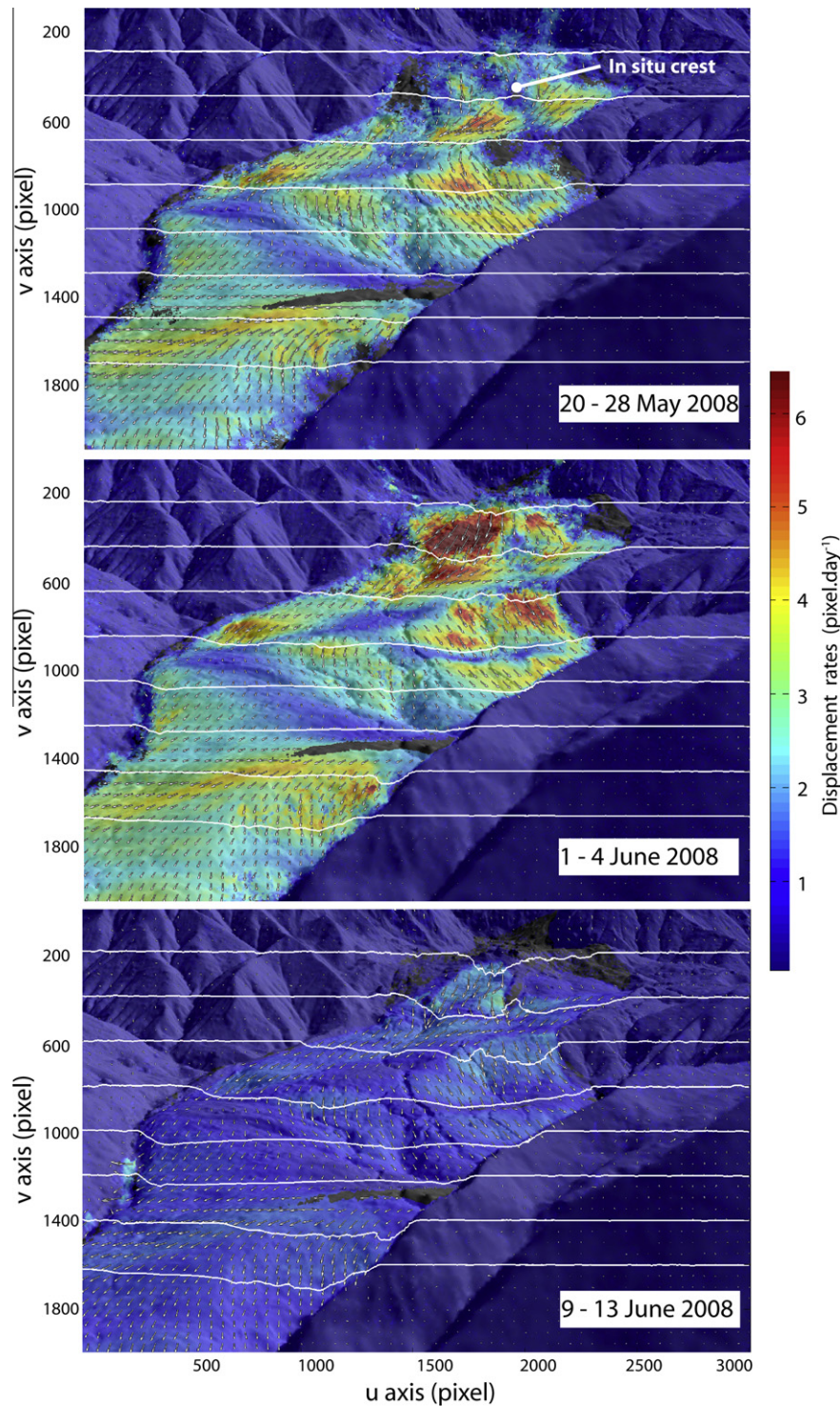
Fig. 6. Displacement rate amplitude (color) and direction (arrow) in the image plane and cumulated displacements along eight profiles crossing the landslide over the period 20 May–25 June 2008. In order to highlight the displacement direction, the arrow length is normalized for each image.

discriminating criterion because some points can display a high correlation coefficient even if they do not represent the same object (e.g. two trees or large stones having the same geometry; Casson et al., 2005).

2. The value of displacement amplitude and direction: points characterized by upslope displacement and important displacement amplitude with reference to a priori knowledge on the landslide kinematics are filtered.

3. The displacements assigned to invisible points from the camera viewpoint because of small orthorectification errors in the conversion to the local coordinate system.

The amount of filtered correlated points varies greatly according to the season; a test carried out with images pairs of 23–27 July 2008 (summer season) and 19–23 October 2008 (autumn season) indicates a number of remaining point post-filtering of
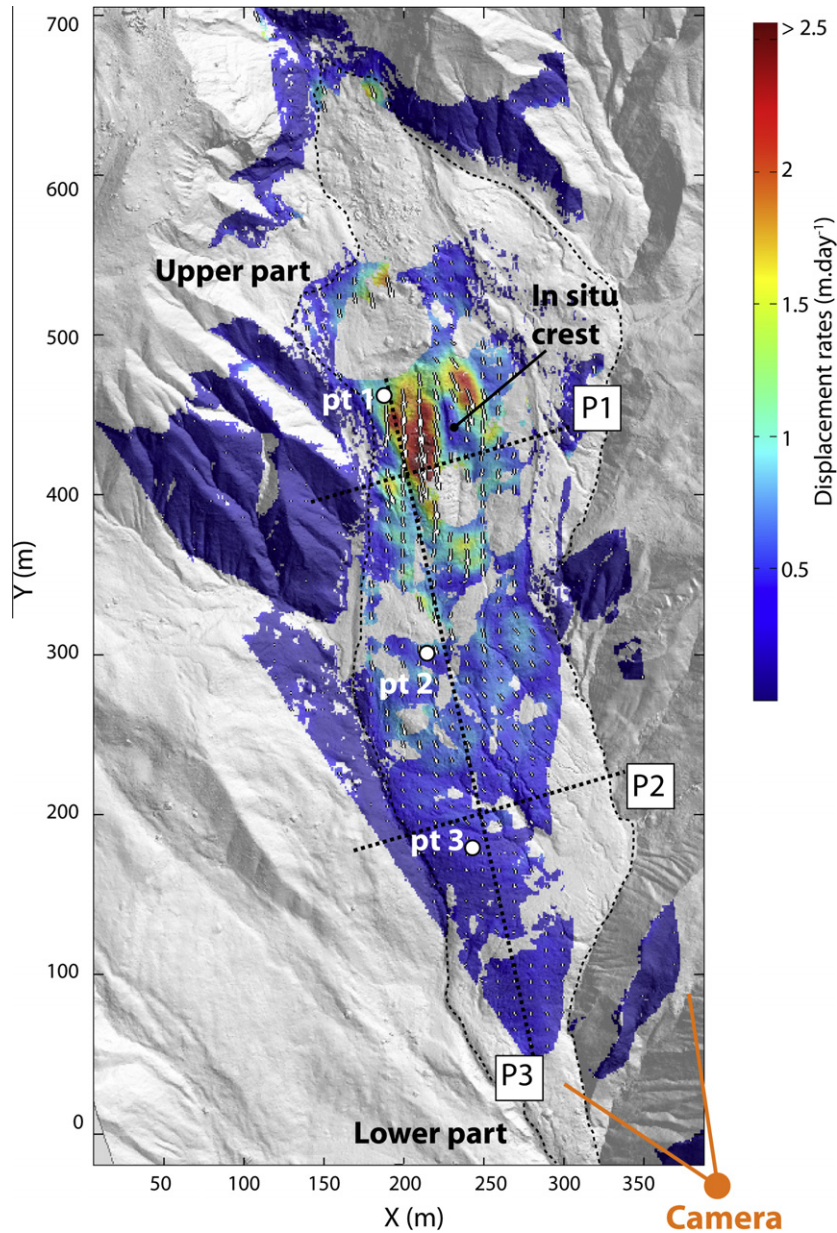
Fig. 7. Displacement rates for the period 1–4 June 2008. The profiles P1, P2 and P3 refer to Fig. 8 and the locations pt 1, pt 2 and pt 3 refer to Fig. 12.

80–90% for the summer period and of only 50% for the autumn period. This is mainly explained by the different illumination conditions (especially low sun elevations in autumn) which affect the quality of the correlation. This aspect will be discussed further in Section 6.1.3.

The upper part of the landslide is most affected by the filtering. This area generally shows a percentage of remaining values lower than in the middle and lower parts of the landslide. This is explained by the fact that the upper part has a more chaotic morphology. Consequently the effects of illumination changes are more important than in the middle and the lower parts, especially in autumn. In addition, the angle of incidence in this area can be low (5–10°) and thus sensitive to slight movements of the camera.

4. Results

4.1. Displacement maps of the landslide

A set of images over the period May–July 2008 is used to illustrate the potential of the technique for the characterization of the kinematics during an acceleration period triggered by high rainfall amounts and a fast melting of the snow cover.

Fig. 6 shows an example of displacement rate (in pixels day^{-1}) of the ground surface in the image plane derived from image pairs of 20–28 May 2008, 1–4 June 2008 and 9–13 June 2008. The reference is the image of 20 May 2008. The contrast in displacement rates between the landslide area and the stable area gives confidence on the calculated velocity field. One can notice that the
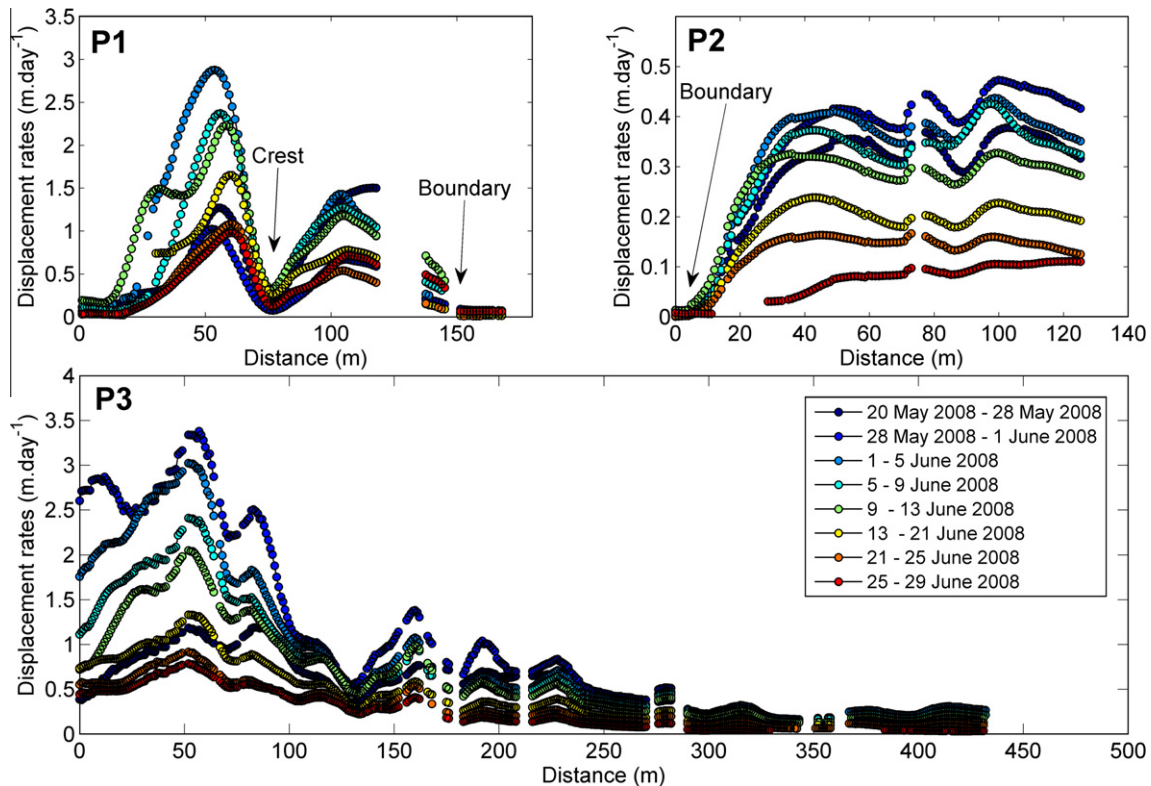
Fig. 8. Profiles of displacement rates in the upper (P1), middle (P2) and lower (P3) parts of the landslide. The location of the profiles is indicated in Fig. 7.

pattern of displacement rate is heterogeneous spatially and temporally. The upper part of the landslide displays the highest velocity ranging from 1 to 7 pixels day^{-1} while the lower part displays velocity of less than 4 pixels day^{-1}. No quantitative comparisons can be carried out at this stage because the pixel sizes vary strongly in the image (Fig. 5A). From the 20 May 2008 to the 13 June 2008, cumulated displacements of up to 110 pixels are observed in the upper part. The maximum displacement rate is observed around the 1st June. Then the landslide decelerates to a displacement rate of about 1 pixel day^{-1}.

Some local specific displacement patterns are also clearly highlighted. For instance, the presence of a stable *in situ* crest located in the landslide body is perfectly identified in the correlated images.

Fig. 7 presents the amplitude of the 3D orthorectified displacement rates for the period 1–4 June 2008 in the local coordinate system. The difference of kinematics between the upper (up to 3 m day^{-1}) and the lower (up to 1 m day^{-1}) parts becomes more evident than in the image plane. The geometrical effect induced by the presence of the stable *in situ* crest on the landslide kinematics is also clearly pointed out. The temporal evolution of the displacement rates is illustrated with two transversal profiles and one longitudinal profile on Figs. 7 and 8. In particular, the difference of displacement rates between the upper and the lower part of the landslide is pointed out.

The precision of the computed displacements is assessed by testing a null hypothesis on the stable areas (Berthier et al., 2005; Casson et al., 2003). Only the points with a correlation coefficient $r > 0.8$ are taken into account. In the image plane coordinate system, the average error μ ranges from 0.5 to 0.9 pixels with standard deviation σ of 0.3 to 1.2 pixels for the image pairs between 20 May 2008 and 25 June 2008. In the local coordinate system, the average error μ ranges from 0.03 to 0.11 m with standard deviation σ of 0.10–0.31 m for the image pairs between 20 May 2008 and 25 June 2008.

4.2. Comparison with dGPS displacements

Sixty benchmarks distributed in the stable parts and on the landslide body were monitored by dGPS (horizontal and a vertical average accuracy of ±0.02 and ±0.05 m) to estimate the accuracy and validate the displacements obtained from image correlation. In total, 219 dGPS measurements are available for the period 2008–2009. In order to validate the displacements computed in the image plane, the dGPS benchmarks are projected to the image plane using the collinearity equations. The pixel displacements derived by image correlation are then averaged in a perimeter of 16 pixels around each benchmark. The results are presented in Fig. 9A. A correlation coefficient of $r = 0.98$ is found between dGPS measurements and image correlation, and an average relative accuracy of 11% is determined (Fig. 9C). In order to validate the metric displacements in the local coordinate system, the orthorectified displacements are averaged in an area of 4 m^2 around each benchmark and compared with the dGPS displacements. A correlation coefficient of $r = 0.95$ is found (Fig. 9B), and an average relative accuracy of 20% is determined (Fig. 9D). The reason why the correlation coefficient in the orthorectified case is lower than in the pixel case is believed to be related to the accuracy of the DEM used for orthorectification. This will be discussed in Section 5.2.2.

5. Discussion: sources of errors

The major sources of errors affecting the displacement calculations and thus limiting the efficiency of TOP for an operational landslide monitoring can be classified in two groups: (i) the parameters affecting the image correlation computation and (ii) the external parameters influencing the orthorectification procedure.
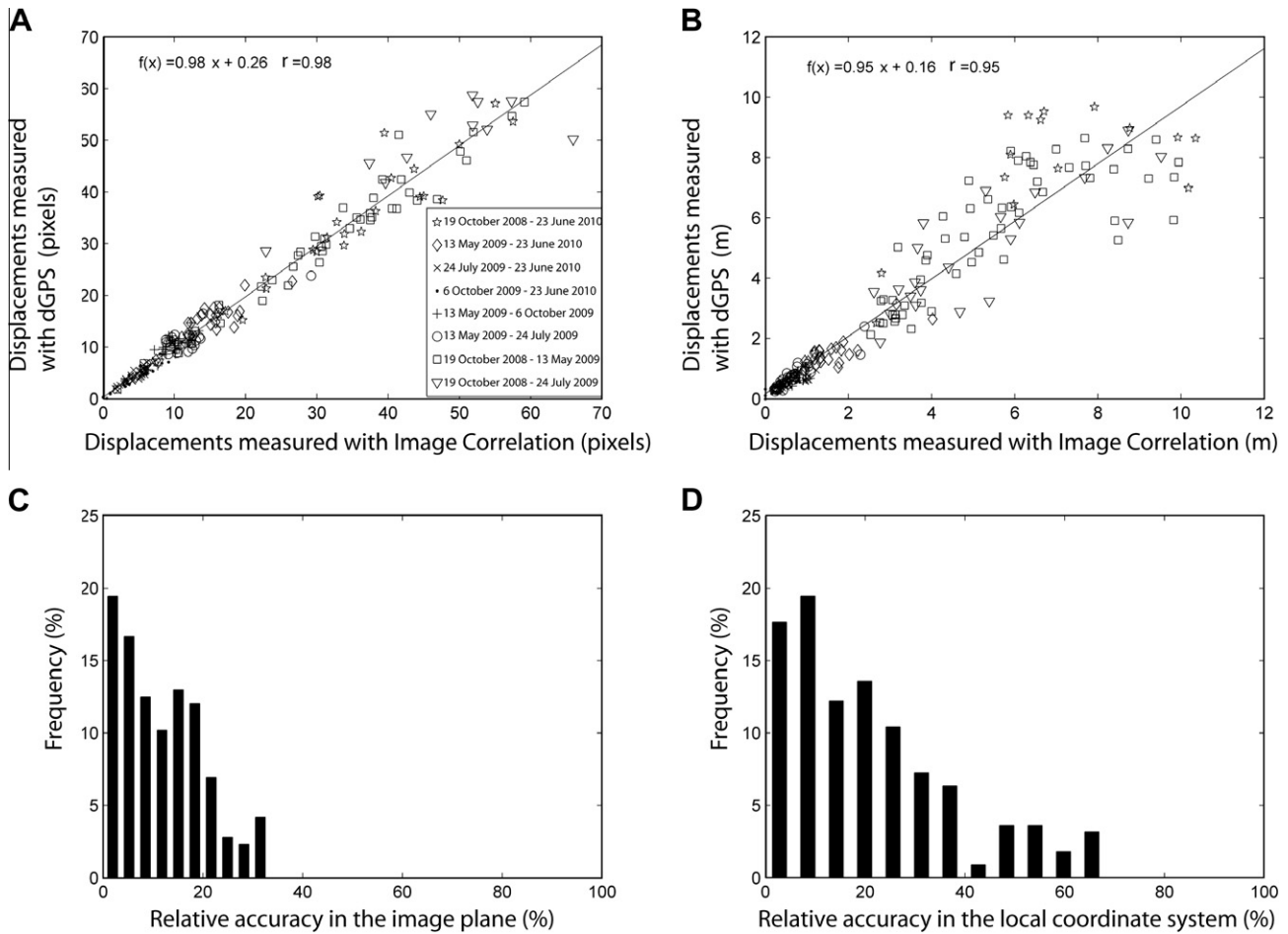
Fig. 9. Assessment of the accuracy of the image correlation technique. Relationships between the displacements observed by image correlation and the displacements measured by dGPS on sixty benchmarks in the image plane (A) and in the local coordinate system (B). Relative accuracy of the image correlation technique in the image plane (C) and in the local coordinate system (D).

5.1. Sources of errors affecting the image correlation computation

5.1.1. Accuracy and precision of the image correlation algorithm

One limitation of the image correlation technique is directly linked to the correlation algorithm and the sub-pixel interpolation method (Debella-Gilo and Kääb, 2011). A series of experimental tests were carried out to assess the precision of the image correlation technique. The series of tests allow one to investigate the influence of the size of the correlation window and of the level of noise observed in the images. Homogeneous imposed displacements (systematically equal to a multiple of pixels to avoid image resampling; Chambon et al., 2003) are applied to pairs of images to create synthetic images. Furthermore, three levels of Gaussian noise were added to the original images with a mean noise level of zero and variances σ^2 of 10^{-4}, 10^{-3} and 10^{-2} (Fig. 10A). Then the image correlation technique is applied to the original image taken as reference and to the synthetic image with different sizes of correlation windows (5, 10, 16, 20, 30 and 50 pixels). For each correlation window, fifteen imposed displacements were calculated with amplitudes ranging from 1 to 23 pixels along the u and v-directions. The analysis was conducted by comparing the noisy synthetic images with the reference image. In the optimal case, the measured displacement would be identical to the imposed displacement.

Each image correlation analysis revealed displacement differences distributed close to zero (mean accuracy of 5×10^{-4} pixels). As observed by Hild (2003), the precision of the correlation

algorithm mainly depends on the pixel fraction of the displacement. Larger correlation windows produce less scattered displacements and therefore improve the precision. By plotting the standard deviation of the calculated displacements against the size of the correlation window, the influence of the correlation window size can be pointed out (Fig. 10B). For very low level of noise, the precision is less than 0.1 pixels for a size of correlation window greater than 5×5 pixels. For higher level of noise, the precision is more dependent on the size of the correlation window. As homogenous displacement fields were imposed to the image, the accuracy (average misfit) is similar for small and large correlation windows. In reality, the displacement field becomes more heterogeneous at higher resolution. Therefore, an increase of the size of the correlation window implies a decrease of the spatial resolution but, as shown in these tests, an increase of the precision.

5.1.2. Influence of ground surface state

The time lag between two image acquisitions is one of the critical factors that affect the correlation computation. This time has to be long enough to increase the signal (e.g. landslide displacement) but short enough to preserve the tracked features (Berthier et al., 2005). Loading of the snowpack on the ground during winter, surface erosion due to fast snow melting and the development of water-saturated ponds in spring, weathering of the objects, growing of grass and large deformations are environmental processes that significantly modify the surface state during a year. Such correlation error sources are characterized by very low correlation
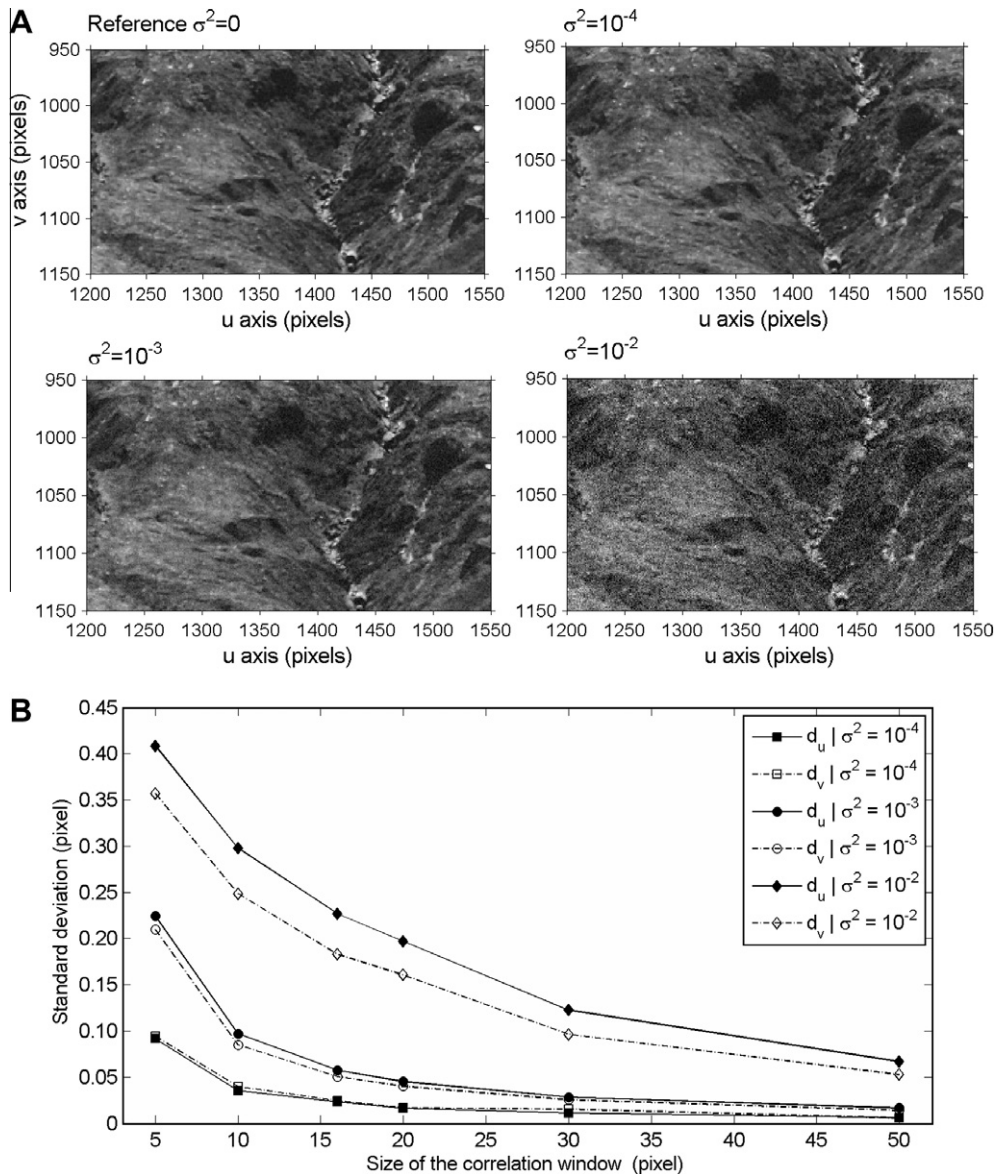
Fig. 10. Precision of the correlation algorithm. (A) Examples of different level of Gaussian noise introduced in the images; (B) Precision of the hierarchical correlator in the u and v direction as a function of different levels of Gaussian noise (σ_n^2) and different sizes of the correlation window.

coefficients, very large displacement amplitudes or randomly-distributed displacement directions in comparison to the neighbor pixels (Fig. 11). On average, about 20–25% of the points are usable from one year to the next year (using a correlation window of 16×16 pixels with a correlation coefficient threshold of 0.8). Consequently, the construction of long time series of displacements with the image correlation technique is a difficult task. The range of cumulated displacement rates observed over a period of 16 months (May 2008–September 2009) is illustrated by tracking the displacement at three locations in the upper (pt 1), middle (pt 2) and lower (pt 3) parts of the landslide in the direct vicinity of benchmark measured by dGPS (Fig. 7). In our case, the cumulated displacements of the year 2009 are adjusted on those of 2008 using GCPs measured with dGPS at the vicinity of the points pt 1, pt 2 and pt 3. The monitoring of some benchmarks with geodetic techniques is necessary to combine displacement patterns observed in image pairs acquired over the period May 2008–September 2009 (74 pairs of images). After the acceleration period of spring 2008, the displacement rates are decreasing to relative

constant values of about 0.02 m day^{-1} in the lower and middle parts and 0.05 m day^{-1} in the upper part computed over the period July to October 2008 (Fig. 12).

5.1.3. Influence of illumination conditions

The difference observed in RGB intensities in various images acquired with various solar illumination angles is an important limiting factor essentially in terms of changes of the shadow areas (Berthier et al., 2005). In order to assess the influence of illumination conditions on the image correlation results, two experiments are carried out.

The first experiment consists in correlating images acquired at different times within a day. Four photographs acquired at 11:00, 12:00, 13:00 and 14:00 GMT in a period of low displacements (<0.02 m day^{-1}, August 2009) under clear sky conditions are correlated. The results indicate that illumination changes can lead to an average μ and a standard deviation σ of pixel-level error of $\mu_{1h} = 1.31$ and $\sigma_{1h} = 0.03$, $\mu_{2h} = 1.35$ and $\sigma_2 = 0.12$, $\mu_{3h} = 1.89$ and $\sigma_{3h} = 0.18$ pixel for time-interval acquisition of 1, 2 and 3 h,
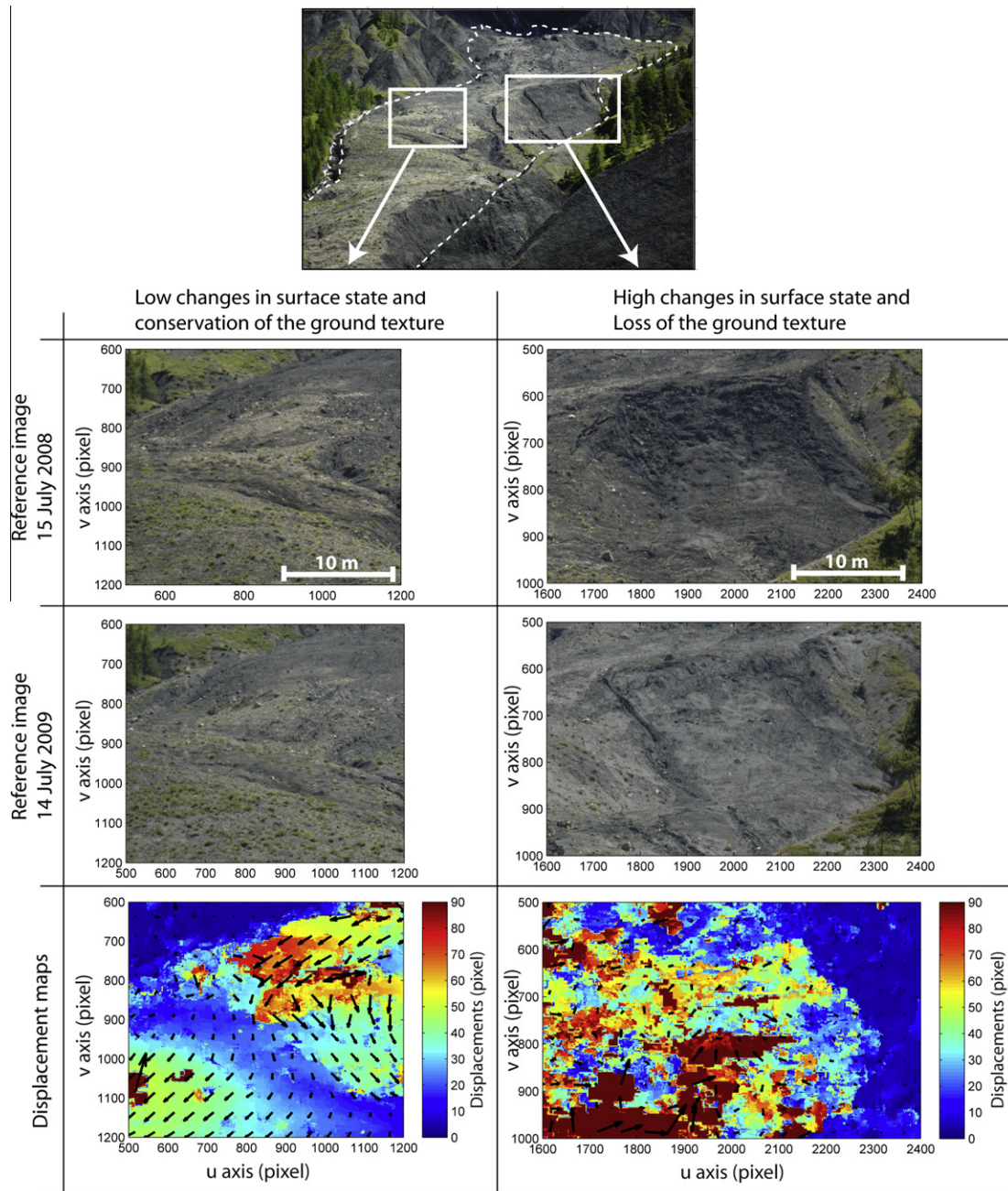
Fig. 11. Example of results for the correlation of two images acquired with one year interval (15 July 2008–14 July 2009), at the same solar time and with clear sky conditions. The incoherency of the displacements is clearly identifiable due to strong surface texture changes (inhomogeneous amplitude and direction of the displacement vectors).

respectively. The results demonstrate that the correlation of images acquired in nearly similar illumination conditions can display a pixel-level precision.

The second experiment consists in creating synthetic images with different shadow intensities as a function of the sun azimuth and elevation (Burrough and McDonnell, 1998). Only the shadows created by direct solar illumination are analyzed assuming clear-sky conditions. The effects of reflected and diffuse illuminations are neglected. Ninety-seven shaded relief images were created with different artificial illuminations (e.g. Fig. 4). Because a preference is given to correlate images taken when the sun elevation is maximal (Delacourt et al., 2007), a shaded relief image with a sun elevation of 65° and a sun azimuth of 250° (illumination coming from the South-West in July at 12:00 GMT) is chosen as the

reference image for the correlation. The reference image is correlated with the shaded relief images. The mean correlation coefficient is used to characterize the influence of illumination changes on the image.

As expected, the correlation of the synthetic images indicates that the correlation coefficient strongly depends on the sun elevation and the sun azimuth (Fig. 13). Illumination coming from the opposite direction of the one of the reference (sun azimuth of 120°) with low elevation angles (<30°; end of the daytime in autumn) provides the less reliable correlation results. This finding is in agreement with Table 2 which indicates that the amount of interpretable displacements is lower in the autumn season than in the summer season (lower correlation coefficients). Therefore, correlation of images with a too large time-lapse has to be avoided
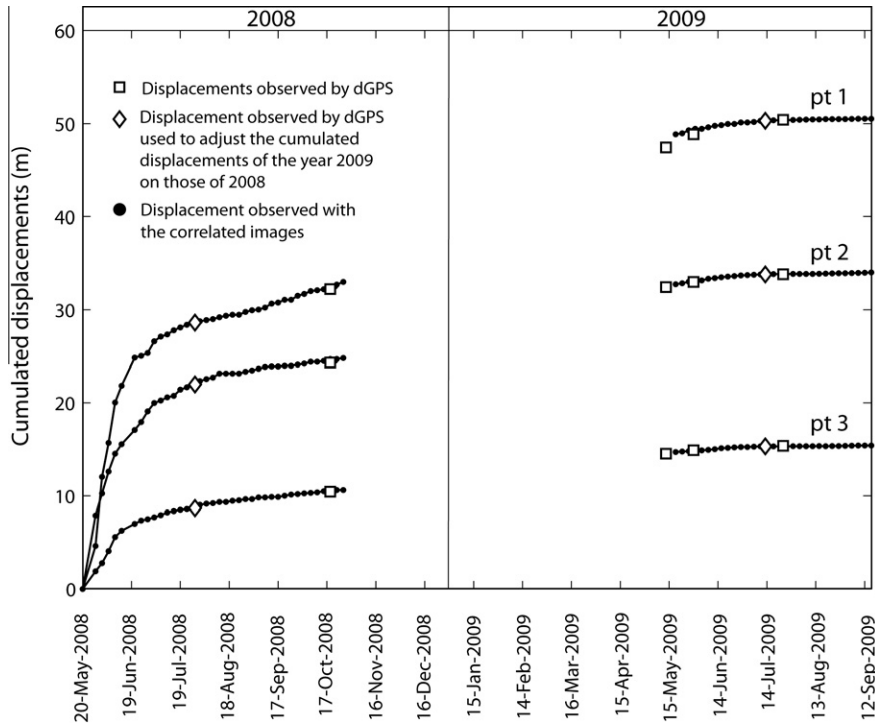
Fig. 12. Cumulated displacements at three locations in the upper (pt 1), middle (pt 2) and lower (pt 3) parts of the landslide. The location of the points is indicated in Fig. 7.
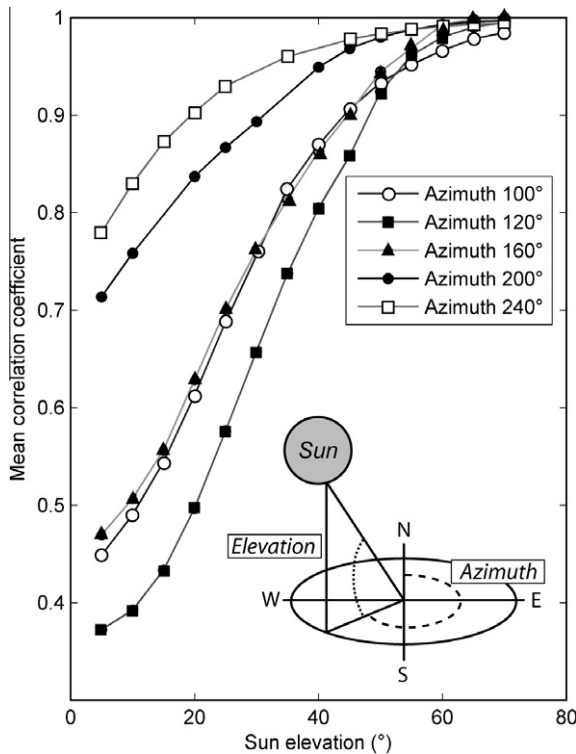
Fig. 13. Influence of illumination conditions as a function of the sun elevation and azimuth on the mean correlation coefficient.

to minimize illumination effects. A possible alternative is to correlate images under diffuse illumination (cloudy day) thus providing a more homogenous lightning. At the opposite, correlation of images acquired at the same solar time during the day and when the sun elevation is maximal is optimal.

In order to compensate for the loss of reliable results in certain areas of the landslide due to strong illumination and ground surface changes, displacements can be interpolated from more reliable neighbor results according to a weight depending on the correlation coefficient (Niebling et al., 2010).

5.2. Sources of errors affecting the ortho-rectification procedure

5.2.1. Influence of camera orientation

The accuracy of the camera orientation is a parameter affecting both the image geometry and the accuracy of the orthorectification (Mikhail et al., 2001). If changes in external orientation of the camera are small, the image geometry is not significantly affected. Consequently a homogeneous component in the correlated displacement field is visible in the image plane (Fig. 14A). This misfit can be significant in the areas where the expected displacements are low or null such as in the stable parts. This systematic error can be corrected assuming a rigid translation of the image by removing the average Δu and Δv misfits (observed on the stable parts of the images such as stable crests or on reference targets located outside the landslide; Fig. 1B and A; Fallourd et al., 2010). Nevertheless this correction is not fully optimal, because the geometric deformations caused by the slight movements of the camera depend on the object distance. Therefore, after correction of the homogeneous component in the image plane, an average residual misfit of about 0–2 pixels is observed.

In order to evaluate the accuracy of the external orientation that influences the orthorectification quality, forty GCPs (not introduced in the minimization processes of Section 3.2.3) are used. The shift between the projected and the observed GCP positions in the image plane is thus determined (Fig. 14B). A mean shift error of −0.20 and −0.08 pixel with a standard deviation of 1.59 and 1.51 pixels, respectively, in the u and v-directions is obtained (Table 3). The accuracy of the external parameters in the orthorectification procedure in the local coordinate system is calculated by comparing the back-projected GCPs identified in the image plane
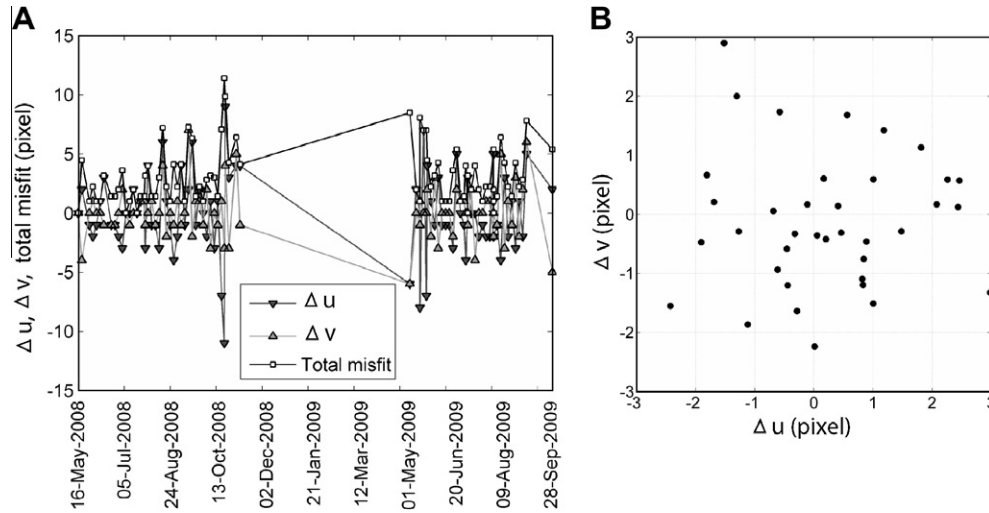
Fig. 14. Assessment of the accuracy of the camera orientation. (A) Average homogenous components due to slight movement of the camera. (B) Residual Δu and Δv misfits between projected and observed GCPs after the least square minimization.

Table 3
Mean value (μ) and standard deviation (σ) of the absolute accuracy for the projection in the image plane and the back-projection in the local coordinate system. n is the number of GCPs used for the calculation of the accuracy.

Image plane (n = 40)	μ (pixel)	σ (pixel)
u	0.20	1.59
v	−0.08	1.51
Local coordinate system (i = 11)	μ (m)	σ (m)
X	0.07	0.41
Y	−0.13	0.53
Z	0.01	0.29

with the GCP positions measured with DGPS and located in the stable parts. The absolute accuracy in X, Y and Z coordinates are presented in Table 3. Because most of GCPs in the stable parts are located in the background of the image where the ground pixel size is about 0.20 m, the mean 3D error (0.14 m) and the standard deviation (0.56 m) of the positioning are not representative of the areas of the landslide located closer to the camera (300 m). Nevertheless, because the standard deviation of the GCPs located in the image plane is close to the accuracy of the GCP picking, the determination of the camera orientation is considered acceptable. Furthermore, the good coherence between the shaded relief images (Fig. 4) and the true images (Fig. 1B) shows that the quality of the determination of the camera orientation is satisfying.

5.2.2. Influence of the DEM

In order to evaluate the influence of the DEM on the orthorectified displacements, the displacements of the period 1–4 June 2008 originally orthorectified with the DEM of October 2007 (Fig. 7) are compared with those orthorectified with the DEM of July 2009 (Fig. 15A and B). The observed differences in displacement are presented relative to the displacement orthorectified with the DEM of 2007. The differences vary spatially in the landslide area. Despite some areas displaying differences in displacement larger than 75%, the average difference is 21% which is very similar to the differences observed with the dGPS measurements (Fig. 9D). As a consequence, the influence of the DEM on the accuracy of the displacement is more important than the influence of the camera orientation, the image resolution and changes in illumination conditions. For large displacements, morphologic changes become significant and the errors on the displacements increase. The computation of multi-temporal DEMs for each image is therefore

a pre-requisite to improve the accuracy of the orthorectified displacements. Nevertheless, in case of a translational landslide characterized by low changes in elevation, the use of the same DEM constitutes still an acceptable 1st-order estimate.

6. Conclusion

The potential of multi-temporal correlation of ground-based images for landslide monitoring has been assessed using the dataset available on the Super-Sauze landslide (South French Alps). A methodology to compute displacement rates both in the image plane coordinate system and in the local coordinate system is proposed.

The results demonstrated clearly the potential and the limitations of this technique by identifying the heterogeneous displacement field of the landslide in space and in time. The camera monitoring allowed to characterize displacements of up to 3 m day^{-1} during an acceleration period, and displacement of about 0.02 m day^{-1} over the decelerating period of July to September. The results are in good agreement with previous knowledge on the landslide kinematics and are in very good agreement with benchmark displacements measured by dGPS.

For objects located in a range of 300–900 m from the camera location, this study showed that the pixel size can vary from 0.005 to 0.04 m^2 according to the resolution of the image (2000 × 3008 pixels) and the angle of incidence of the line of sight. The orientation of the line of sight to the ground surface has to be considered before installing a permanent monitoring system. Areas of low incidence angles (<5°) are very sensitive to small movements of the camera. Therefore, the angle should be as perpendicular as possible to the mean displacement vector of the landslide. 3D displacements of less than 0.04 and 0.06 m in the lower part of the landslide and 0.09 and 0.11 m in the u and v-directions over a period of four days are impossible to detect without the use of sub-pixel correlation algorithms. However, the sources of errors due to small movement of the camera and the use of a mono-temporal DEM are the main limiting factors. A regular acquisition of multi-temporal DEMs through airborne or Terrestrial Laser Scanning or stereoscopic photogrammetric views is believed to be a priority to significantly improve the accuracy of the technique. The errors induced by the sub-pixel correlation algorithm are thus insignificant compared to the influences of the other parameters cited previously.

Fig. 15. Influence of the DEM on the orthorectification of the displacement field. (A) Relative difference between the displacement field of the 1st–4th of June orthorectified with a DEM of 2007 and a DEM of 2009. (B) Histogram of the relative differences.

The results demonstrate that image correlation techniques implemented in permanent monitoring system are particularly interesting for monitoring landslides characterized by annual pluri-decimetric displacements. In addition, this low-cost technique is a very suitable alternative for inaccessible landslides or areas without access to power supply. Furthermore, because the proposed methodology does not require GCPs except for the calibration of the camera and for combining displacement patterns observed in image pairs acquired over two years, the methodology can be routinely and automatically applied to new image pairs. Therefore this work offers very promising perspectives for operational applications which can be potentially integrated in early warning systems by considering additional efforts in direct data transmission. Finally, inversion of the displacement field could be developed to characterize the macroscopic rheological properties of the landslide material.

Acknowledgments

References

Abdel-Aziz, Y.I., Karara, H.M., 1971. Direct linear transformation into object space coordinates in close-range photogrammetry. In: Proc. Symposium on Close-Range Photogrammetric Systems, ASP, Falls Church, VA, 5–10 April, pp. 1–18.

Anandan, P., Bergen, R.J., Hanna, K.J., Hanna, K.J., 1993. Hierarchical model-based motion estimation. In: Sezan, L. (Ed.), Image Sequence Analysis. Kluwer, Dordrecht, pp. 237–252.

Baratoux, D., Delacourt, C., Allemand, P., 2001. High-resolution digital elevation models derived from Viking Orbiter images: method and comparison with Mars Orbiter Laser Altimeter Data. Journal of Geophysical Research 106 (E12), 32927–32941.

Berthier, E., Vadon, H., Baratoux, D., Arnaud, Y., Vincent, C., Feigl, K.L., Rémy, F., Legrésy, B., 2005. Surface motion of mountain glaciers derived from satellite optical imagery. Remote Sensing of Environment 95 (1), 14–28.

Bitelli, G., Dubbini, M., Zanutta, A., 2004. Terrestrial laser scanning and digital photogrammetry techniques to monitor landslides bodies. International Archives of Photogrammetry, Remote Sensing and Spatial Information Sciences 35 (Part B5), 246–251.

Bonneval, H., 1972. Levés topographiques par photogrammétrie aérienne. Photogrammétrie Générale: Tome 3, Collection Scientifique de l'Institut Géographique National, Eyrolles, Paris.

Brunner, F., Macheiner, K., Woschitz, H., 2007. Monitoring of deep-seated mass movements. In: Proceedings of the Third International Conference on Structural Health Monitoring of Intelligent Infra-structure (SHMII-3), Vancouver, Canada, 13–16 November, 7p. (on CDROM).

Burrough, P.A., McDonnell, R.A., 1998. Principles of Geographical Information Systems. Oxford University Press, New York.

Cardenal, J., Mata, E., Perez-Garcia, J.L., Delgado, J., Andez, M.A., Gonzalez, A., Diaz-de-Teran, J.R., 2008. Close-range digital photogrammetry techniques applied to landslide monitoring. International Archives of Photogrammetry, Remote Sensing and Spatial Information Sciences 37 (Part B8) (on CDROM).

Casagli, N., Farina, P., Leva, D., Tarchi, D., 2004. Application of ground-based radar interferometry to monitor an active rock slide and implications on the emergency management. In: Evans, S.G., Scarascia-Mugnozza, G., Strom, A., Hermanns, R.L. (Eds.), Landslides from Massive Rock Slope Failure, Proceedings of the NATO Advanced Research Workshop on Massive Rock Slope Failure – New Models for Hazard Assessment, Celano, Italy, 16–21 June, Springer, Berlin, pp. 351–360.

The strongest limitations are independent of the acquisition system. They are related to the meteorological and illumination conditions and the ground surface changes inducing partial or complete loss of coherence between image pairs. During the winter season (from the months November to May), the presence of snow impedes reliable correlation results while excessive ground displacements between two consecutive years impede valid displacement measurements even if the images are acquired during the same solar time.

Casson, B., Baratoux, D., Delacourt, D., Allemand, P., 2003. Seventeen years of the "La Clapière" landslide evolution analysed from ortho-rectified aerial photographs. Engineering Geology 68 (1–2), 123–139.

Casson, B., Delacourt, C., Allemand, P., 2005. Contribution of multi-temporal sensing images to characterize landslide slip surface – application to the La Clapière Landslide (France). Natural Hazards and Earth System Sciences 5, 425–437.

Chambon, G., 2003. Caractérisation expérimentale du frottement effectif des zones de faille. Ph.D. Thesis, Earth Sciences, Université Paris XI-Orsay, Paris.

Chambon, G., Schmittbuhl, J., Corfdfir, A., Vilotte, J.-P., Rous, S., 2003. Shear with comminution of a granular material: microscopic deformations outside the shear band. Physical Review E 68 (1), 1–8.

Corripio, J.G., 2004. Snow surface albedo estimations using terrestrial photography. International Journal of Remote Sensing 25 (24), 5705–5729.

Corsini, A., Farina, P., Antonello, G., Barbieri, M., Casagli, N., Coren, F., Guerri, L., Ronchetti, F., Sterzai, P., Tarchi, D., 2006. Space-borne and ground-based SAR interferometry as tools for landslide hazard management in civil protection. International Journal of Remote Sensing 27 (12), 2351–2369.

D'Antone, I., 1995. Hierarchical correlation for track finding. Nuclear Instrument and Methods in Physics Research 356 (2–3), 476–484.

Debella-Gilo, M., Kääb, A., 2011. Sub-pixel precision image matching for measuring surface displacements on mass movements using normalized cross-correlation. Remote Sensing of Environment 115 (1), 130–142.

Delacourt, C., Allemand, P., Berthier, E., Raucoules, D., Casson, B., Grandjean, P., Pambrun, C., Varel, E., 2007. Remote-sensing techniques for analysing landslide kinematics: a review. Bulletin de Société Géologique 178 (2), 89–100.

Delacourt, C., Allemand, P., Casson, B., Vadon, H., 2004. Velocity field of the "La Clapière" landslide measured by the correlation of aerial and Quick-Bird satellite images. Geophysical Research Letters 31 (L15619), 1–5.

El Alaoui, M.I., Ibn-Elhaj, E., 2009. A robust hierarchical motion estimation algorithm in noisy image sequences in the bispectrum domain. Signal Image and Video Processing 3 (3), 291–302.

Fallourd, R., Vernier, F., Friedt, J.-M., Martin, G., Trouvé, E., Moreau, L., Nicolas, J.-M., 2010. Monitoring temperate glacier with high resolution automated digital cameras – application to the Argentière Glacier. International Archives of Photogrammetry Remote Sensing and Spatial Information Sciences 38 (Part 3B), 1–23.

Fisher, P.F., 1991. First experiments in viewshed uncertainty: the accuracy of the viewshed area. Photogrammetric Engineering & Remote Sensing 57 (10), 1321–1327.

Foppe, K., Barth, W., Preis, S., 2006. Autonomous permanent automatic monitoring system with robot-tacheometers. In: Proc. XXIII International FIG Congress 'Shaping the Change' (FIG-2006), Münich, Germany, 8–13 October, 12p. (on CDROM).

Franklin, W.R., Rav, C.K., 1994. Higher isn't necessarily better: visibility algorithms and experiments. In: Waugh, T.C., Healey, R.G. (Eds.), Proceedings of the Sixth International Symposium on Spatial Data Handling 'Advances in GIS Research' (SDH'94), Edinburgh, Scotland, vol. 2. Taylor & Francis, London, pp. 751–770.

Heikkila, J., Silven, O., 1997. A four-step camera calibration procedure with implicit image correction. In: Proceedings of the IEEE Computer Society Conference on Computer Vision and Pattern Recognition (CVPR'97), San Juan, Puerto Rico, 17–19 June, pp. 1106–1112.

Hemmleb, M., Wiedemann, A., 1997. Digital rectification and generation of orthoimages in architectural photogrammetry. International Archives of Photogrammetry and Remote Sensing 32 (Part 5C1B), 261–267.

Hild, F., 2003. Mesure de champs de déplacement par corrélation d'images et applications en mécanique des solides. Notes de Cours IPSI. Laboratoire de Mécanique et de Technologie, Université Paris 6, France.

Honda, K., Nagai, M., 2002. Real-time volcano activity mapping using ground-based digital imagery. ISPRS Journal of Photogrammetry and Remote Sensing 57 (1–2), 159–168.

Jaboyedoff, M., Oppikofer, T., Abellan, A., Derron, M.-H., Loye, A., Metzger, R., Pedrazzini, A., 2010. Use of LiDAR in landslide investigations: a review. Natural Hazards 2010, 1–24. http://dx.doi.org/10.1007/s11069-010-9634-2.

Jaboyedoff, M., Ornstein, P., Rouiller, J.-D., 2004. Design of a geodetic database and associated tools for monitoring rock-slope movements: the example of the top of Randa rockfall scar. Natural Hazards and Earth System Science 4, 187–196.

Jiang, R., Jauregui, D.V., White, K., 2008. Close-range photogrammetry applications in bridge measurement: literature review. Measurement 41 (8), 823–834.

Kraus, K., Waldhäusl, P., 1994. Photogrammetry: Fundamentals and Standard Processes. Hermès, Paris.

Kumar, S., Banerjee, S., 1998. Development and application of a hierarchical system for digital particle image velocimetry to free-surface turbulence. Physics of Fluids 10 (1), 160–177.

Küntz, M., Jolin, M., Bastien, J., Perez, F., Hild, F., 2007. Digital image correlation analysis of cracks behavior in a reinforced concrete beam during a load test. Canadian Journal of Civil Engineering 33 (11), 1418–1425.

LePrince, S., Berthier, E., Ayoub, F., Delacourt, C., Avouac, J.-P., 2008. Monitoring earth surface dynamics with optical imagery. EOS Transactions 89 (1), 1–5.

Lewis, J.P., 1995. Fast normalized cross-correlation. Vision Interface 10 (1), 120–123.

Lim, M., Petley, D.N., Rosser, N.J., Allison, R.J., Long, A.J., Pybus, D., 2005. Combined digital photogrammetry and time-of-flight laser scanning for monitoring cliff evolution. The Photogrammetric Record 20 (110), 109–129.

Maas, H.-G., Schwalbe, E., Dietrich, R., Bässler, M., Ewert, H., 2008. Determination of spatio-temporal velocity fields on glaciers in West-Greenland by terrestrial image sequence analysis. International Archives of Photogrammetry, Remote Sensing and Spatial Information Science 37 (Part B8), 1419–1424.

Malet, J.-P., 2003. Les glissements de type écoulement dans les marnes noires des Alpes du Sud. Morphologie, fonctionnement et modélisation hydromécanique. Ph.D. Thesis, Earth Sciences, Université Louis Pasteur, Strasbourg.

Malet, J.-P., Maquaire, O., Calais, E., 2002. The use of global positioning system techniques for the continuous monitoring of landslides. Geomorphology 43 (1–2), 33–54.

Mikhail, E., Bethel, J.S., McGlone, J.C., 2001. Introduction to Modern Photogrammetry. John Wiley & Sons Inc., New York.

Monserrat, O., Crosetto, M., 2008. Deformation measurement using terrestrial laser scanning data and least squares 3D surface matching. ISPRS Journal of Photogrammetry and Remote Sensing 63 (1), 142–154.

Naterop, D., Yeatman, E., 1995. Automatic measuring system for permanent monitoring: solexperts geomonitor. Proceedings of 4th International Symposium on Field Measurements in Geomechanics (FMGM-1995), Bergamo, 18–23 April, pp. 417–424.

Niebling, M.J., Flekkøy, E.G., Måløy, K.J., Toussaint, R., 2010. Mixing of a granular layer falling through a fluid. Physical Review E 82 (1), 1–16.

Oppikofer, T., Jaboyedoff, M., Kreusen, H.-R., 2008. Collapse at the eastern Eiger flank in the Swiss Alps. Nature Geoscience 1 (8), 531–535.

Pesci, A., Baldi, B., Bedin, A., Casula, G., Cenni, N., Fabris, M., Loddo, F., Mora, P., Bacchetti, M., 2004. Digital elevation models for landslide evolution monitoring: application on two areas located in the Reno River Valley (Italy). Annals of Geophysics 47 (4), 1339–1353.

Press, W.H., Flannery, B.P., Teukolsky, S.A., Vetterling, W.T., 1997. Numerical Recipes. Cambridge University Press, New York.

Rohály, J., Frigerio, F., Hart, D.P., 2002. Reverse hierarchical PIV processing. Measurement Science and Technology 13 (7), 984–996.

Squarzoni, C., Delacourt, C., Allemand, P., 2005. Differential single-frequency GPS monitoring of the La Valette landslide (French Alps). Engineering Geology 79 (3–4), 215–229.

Sturzenegger, M., Stead, D., 2009. Close-range terrestrial digital photogrammetry and terrestrial laser scanning for discontinuity characterization on rock cuts. Engineering Geology 106 (3–4), 163–182.

Tarchi, D., Casagli, N., Fanti, R., Leva, D.D., Luzi, G., Pasuto, A., Pieraccini, M., Silvano, S., 2003. Landslide monitoring by using ground-based SAR interferometry: an example of application to the Tessina landslide in Italy. Engineering Geology 68 (1–2), 15–30.

Teza, G., Galgaro, A., Zaltron, N., Genevois, R., 2007. Terrestrial laser scanner to detect landslide displacement fields: a new approach. International Journal of Remote Sensing 28 (16), 3425–3446.

Teza, G., Pesci, A., Genevois, R., Galgaro, A., 2008. Characterization of landslide ground surface kinematics from terrestrial laser scanning and strain field computation. Geomorphology 97 (3–4), 424–437.

Travelletti, J., Malet, J.-P., 2012. Characterization of the 3D geometry of flow-like landslides: a methodology based on the integration of multi-source data. Engineering Geology 128, 30–48.

Wangensteen, B., Guomundsson, A., Eiken, T., Kääb, A., Farbrot, H., Etzelmüller, B., 2006. Surface displacements and surface estimates for creeping slope landforms in Northern and Eastern Iceland using digital photogrammetry. Geomorphology 80 (1–2), 59–79.

White, D.J., Take, W.A., Bolton, M.D., 2003. Soil deformation measurement using particle image velocimetry (PIV) and photogrammetry. Géotechnique 53 (7), 619–631.